13

Probe microscopy of resistive switching in nanocrystalline copper oxide (Cu_xO)

© L.Yu. Fedorov,[1,2] I.V. Karpov,[1,2] A.V. Pavlov,[1,2] A.M. Zhilkashinova,[3] A.I. Lyamkin[1,2]

[1]Krasnoyarsk Scientific Center of the Siberian Branch of the Russian Academy of Sciences,
660036 Krasnoyarsk, Russia
[2]Siberian Federal University,
660041 Krasnoyarsk, Russia
[3]Sarsen Amanzholov East Kazakhstan University,
070002 Ust-Kamenogorsk, Kazakhstan
e-mail: 1401-87@mail.ru

Received April 23, 2025
Revised April 23, 2025
Accepted April 23, 2025

The paper studies the effect of resistive switching in nanocrystalline copper oxide (Cu_xO) films synthesized by vacuum arc deposition in an argon-oxygen atmosphere. The structural and electrophysical properties of films with different phase compositions (Cu_2O, CuO, mixed phases) are studied using X-ray diffraction, Raman and photoluminescence spectroscopy, and atomic force microscopy. It is found that changing the partial pressure of oxygen during synthesis allows one to control the stoichiometry and defect structure of oxides. Conductive atomic force microscopy modes are used for local analysis of resistive switching, demonstrating bipolar behavior for mixed Cu_xO phases. The results confirm the promise of nanocrystalline copper oxides for creating memristors with controlled characteristics.

Keywords: copper oxides, stoichiometry, vacuum arc, memristors.

DOI: 10.61011/TP.2025.10.62080.74-25

Introduction

Resistive switching (RS) effect is a reversible dielectric thin layer breakdown. It is at the base of operation of devices referred to as memristors (memory resistivity) [1]. Variability of electrical resistance between stable states under the action of an electric field is one of the requirements for memristors. Considerable focus was made on investigating dielectric hafnium, tantalum, zirconium oxides, a number of transition metal (copper, nickel, etc.) oxides having a semiconductor nature. Such materials often use filamentary conductivity variation mechanism to explain the RS effect. It is related to formation of an active oxygen or metal ion vacancy chain layer (conductive bridge) to provide current flow when a cell is turned on.

Features of filament formation and break depend on the nature of conductivity of binary oxide (*p*- or *n*-type), and active or inert electrodes. A conductive bridge in a dielectric layer may be represented by active electrode atoms according to an electrochemical metallization or positively charged vacancy migration mechanism.

Application of reverse voltage (for bipolar switching) causes dissociation of the memristor conductive channel and a corresponding increase in resistance — OFF state of the cell. Disadvantages of the filamentary mechanism include stochastic formation of the conductive channel [2]. This limits the resistive state formation stability.

Many researchers considered using CuO as a candidate for next generation memory devices [3 and references therein]. Most studies used compounds abundant in intrinsic defects to investigate resistive switching in copper oxides. Oxides with stoichiometry deviation both in copper and oxygen were analyzed to enable control of the amount of cations, cation and oxygen vacancies [4–7]. Effective switching with a broad window between states may be achieved by combining the electrode type and oxide layer composition. In copper oxide, this is facilitated by high copper ion diffusion rate in diffusion channels formed by grain boundaries. These processes were well studied when explaining the nanowire growth mechanism on the oxide surface under the action of temperature. In this case, the copper base is the source of ions transported to the CuO surface through an intermediate Cu_2O layer. [8] Taking into account these features, a memristor interconnect layer may be formed in a targeted way for filament formation ordering. This also explains why an active lower electrode made from copper is often chosen. Modern studies emphasize that not merely the density of defects, but the spatial correlation of defects is the key property for RS in Cu_xO.

The purpose of this study is to investigate the effect of phase composition and defect structure of copper oxides on the resistive switching properties. A nanocrystalline film consisting of mixed copper oxide phases (Cu_xO) is examined in this work. The film features a higher density of structural defects compared with stoichiometric oxides.

1. Experimental procedure

Formation of thin oxide films took place during vacuum arc sputtering [9,10] of metallic copper in argon/oxygen atmosphere followed by deposition onto prepared silicon wafers. Arc discharge current was 90 A, operating pressure was 1 Pa, a gas puffing system provided injection of reaction gas (1−20 vol.% O_2) and buffer gas (Ar) for plasma-chemical reactions. Wafers were heated to 200 °C during the deposition.

Three types of oxide films were prepared. Sample 1 with prevailing Cu_2O phase and metallic copper inclusion, sample 2 and sample 3 were prepared at a partial oxygen pressure corresponding to injection of 1 vol.% O_2, −5 vol.% O_2 and −20 vol.% O_2, respectively. The samples were not subjected to further annealing.

Powder diffraction data was obtained at room temperature using the Bruker D8 Advance diffractometer with CuK_α radiation ($\lambda = 0.1540$ nm) and a linear detector. The step angle2θ was 0.01°, the count time was — 0.2 s per step angle. Analysis of the crystal structure on experimental X-ray patterns used the PDF-4+ data provided by the International Centre for Diffraction Data (ICDD).

Raman scattering spectroscopy was performed on the EnSpectr V532 Raman express analyzer at room temperature. Laser wavelength — 532 nm, spectral resolution — 4−6 cm^{-1}, sampling range — 160−4000 cm^{-1}.

Photoluminescence spectra at room temperature were recorded using the Fluorolog (Horiba Jobin-Yvon) with excitation by a 355 nm (3.49 eV) xenon short-arc lamp.

Atomic force microscopy investigations used the SMM-2000 scanning probe microscope („Proton“, Russia). Contact potential difference (CPD) of the samples was measured by DC-biased Kelvin probe force microscopy (DC-KPFM) using the PFQNE-AL cantilevers (Bruker) with the nominal resonance frequency of 300 kHz and hardness of 0.8 N/m. Gold contacts were used for calibration of the probe work function. Thirty measurements per sample were carried out in various random positions with truncation of extreme CPD values. The resistive switching effect was studied in the conductive atomic force microscopy (CAFM) mode. Scanning field was $2.1 \times 2.1\,\mu$m (512×512 pixels). AFM image processing was performed using SMM-2000 analysis software supplied with the microscope.

On a separate note, the quality of electric contact between the probe and sample in the CAFM mode has a key effect on the accuracy and interpretation of local VAC measurements. Therefore, the following procedures were implemented to provide this contact:

- Using Golden Silicon Probes CSG01 with a tip radius of 35 nm and conductive PtIr coating to provide stable ohmic contact with oxide film surface. PtIr was chosen due to its high resistance to electrochemical processes and stable work function close to the value with Fermi levels of the Cu_xO phases of interest (5.1−5.4 eV).
- Prior to the measurement series, the cantilevers were brought into test contact with the reference metal sample (gold) to identify probes with damaged or oxidized coating.
- Cantilever load was set to the lowest possible value to avoid contact degradation.
- To minimize possible spurious electrochemical processes, measurements were performed in dry atmosphere at room temperature, with short voltage supply and current limiting time intervals to prevent local overheating.
- Main VAC measurements were performed within ±6 V, which is lower than the detectable surface oxidation threshold for PtIr probes and Cu_xO.
- Areas with a minimum conductive spot diameter, where the filament is formed in an area comparable with the probe radius, were investigated. This reduces the probability of uneven field distribution.

The chosen voltage conditions didn't induce any observable surface degradation effects (for example, plastic strains, anodic oxidation traces, etc.), which also confirms the contact stability. Thus, this work implemented a strategy of minimizing the spurious contact effects and of „probe-sample“ connection stability control to provide reliable detection of local resistive transitions and their hysteresis behavior.

RS AFM test samples consisted of standard p-Si (001) wafers coated with a SiO_2 (~ 500 nm) layer as a substrate. The lower electrode consisted of a Cu (100 nm) layer deposited by a magnetron sputtering technique. Active layer was a polycrystalline film consisting of mixed copper oxide phases formed by the vacuum-arc sputtering technique. Cu_xO layer thickness was estimated as ~ 30 nm and was controlled by the time of wafer exposure to plasma cloud. The probe microscope cantilever served as the upper electrode.

2. Findings and discussion

Figure 1 shows X-ray images of the prepared copper oxide films. Successive increase in the partial oxygen pressure during preparation of each of the samples leads to various degrees of copper oxidation to form the corresponding crystalline Cu_2O and CuO phases. Sample 1 deposited at low PO_2 shows the main diffraction peaks at $2\theta = 29.7$, 36.5, 42.4, 52.7, 61.6 and 73.9° that may be referred to the Cu_2O phase [PDF-4+ № 78-2076] with a cubic crystalline structure. In Cu_2O, copper has oxidation degree (I) and each Cu^+ of the lattice cell is coordinated by two oxygen ions. Corresponding reflection lattice planes are shown in Figure 1. The X-ray pattern of sample 1 also has diffraction peaks at $2\theta = 43.4$ and 50.5° corresponding to metallic copper with a face-centered cubic lattice [PDF-4+ 01-085-1326].

Sample 2 is characterized by the presence of mixed copper oxide phases. Besides the above-mentioned Cu_2O peaks, there are reflections from lattice planes of monoclinic CuO at 35.6, 38.6 and 48.8° [PDF-4+ № 45-0937]. Further

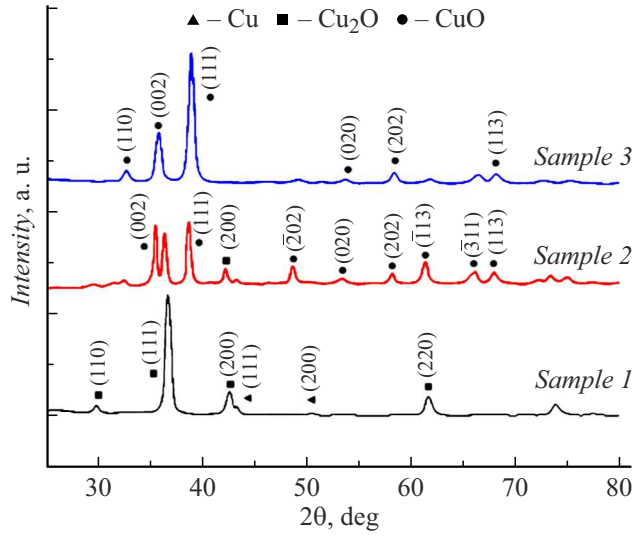

Figure 1. X-ray diffraction patterns of copper oxides deposited with oxygen concentration of: 1 vol.% (sample 1), 5 vol.% O_2 (sample 2), 20 vol.% O_2 (sample 3).

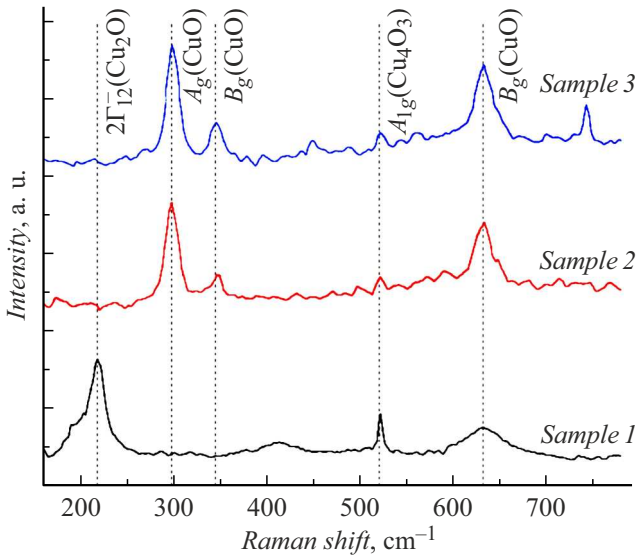

Figure 2. Raman spectra of copper oxides deposited with oxygen concentration of: 1 vol.% (sample 1), 5 vol.% O_2 (sample 2), 20 vol.% O_2 (sample 3).

change in oxide film formation conditions leads to full conversion of the Cu_2O phase into the CuO phase with a monoclinic lattice where Cu^{2+} ions are fourfold coordinated by oxygen (sample 3).

Phase composition variation depending on the synthesis conditions (partial oxygen pressure) was investigated using the Raman scattering spectroscopy. Figure 2 shows the Raman spectra of all test samples. Peaks at 218 and 621 cm^{-1} correspond to the Cu_2O phase. An additional peak at 521 cm^{-1} is assigned to Cu_4O_3, which is a chemical and structural intermediate compound of CuO and Cu_2O. Peaks at 298, 345 and 632 cm^{-1} refer to the CuO phase [11,12]. When oxides are prepared, copper successively undergoes a change in the oxidation degree in the $Cu \rightarrow Cu_2O \rightarrow Cu_4O_3 \rightarrow CuO$ series. In this respect, the Cu_4O_3 and Cu_2O phases are suboxide, but Cu_2O is a stable phase where each Cu^+ of the lattice cell is coordinated by two oxygen ions, and Cu_4O_3 is a metastable state. Cu_4O_3 may be described as a phase originating from the CuO structure by removing oxygen atoms.

Spectrum of sample 1 demonstrates peaks at 218 and 621 cm^{-1}, which confirms that the Cu_2O phase was formed during the synthesis. When the oxygen percentage is increased to 5 %, CuO peaks with a small Cu_2O peak are observed in sample 2. With further increase in the oxygen percentage to 20 %, the spectrum for sample 3 showed CuO peaks with higher intensity. Active Raman modes in Cu_xO include only oxygen movement [12]. Thus, a decrease in Raman peak intensity may be an indirect evidence of the presence of oxygen vacancies during oxide synthesis in oxygen-deficient atmosphere.

Photoluminescent spectroscopy, that is able to differentiate contribution of each type of defect to radiation, is one of the effective techniques used to identify impurity and defect states of semiconductor material crystal structures. It has a high sensitivity, detecting impurities and defects in a concentration range of $10^{-5} - 10^{-7}$ at.%. Photoluminescence in copper oxides is defined by complex interaction of interband transitions (exciton series for Cu_2O, direct/indirect transitions for CuO), defect states (copper/oxygen vacancies, grain boundaries) and quantum-size effects. Defect-induced radiation bands in coper oxides result from occurrence of traps for charge carriers within the band gap, modifying the band structure. Behavior of electron-hole pair transfer and recombination processes between states defines spectral characteristics of photoluminescence (PL). Section 2 described the main types of defects typical for copper oxides, electron structure and the effect of defects on optical properties.

Previous measurements of the Hall effect performed using the Van der Pauw method [13] for the same samples showed that films with all compositions demonstrate the *p*-type conductivity behavior induced by negatively charged copper vacancies. Band gap of copper oxide films evaluated by the Tauc method in the same study was as follows: 1.34 eV for samples with the CuO phase; $\sim$ 1.87 eV in a sample containing mixed two-phase CuO/Cu_2O crystal structure, which is close to 1.9 eV of sample 1 with the Cu_2O phase. Defects related to the absence of copper atoms in the lattice form deep acceptor levels in the band gap. These states capture electrons, facilitating slow recombination processes and induce PL in blue and green ranges (400–550 nm, 2.2–3.1 eV).

Figure 3, *a* shows normalized PL spectra of samples 1 and 2 measured at room temperature with 3.49 eV ($\lambda = 355$ nm) photon excitation. The spectrum of sample 1 consisting of Cu_2O has a sharp asymmetric band with the center near 2.0 eV. Cu_2O luminescence was extensively

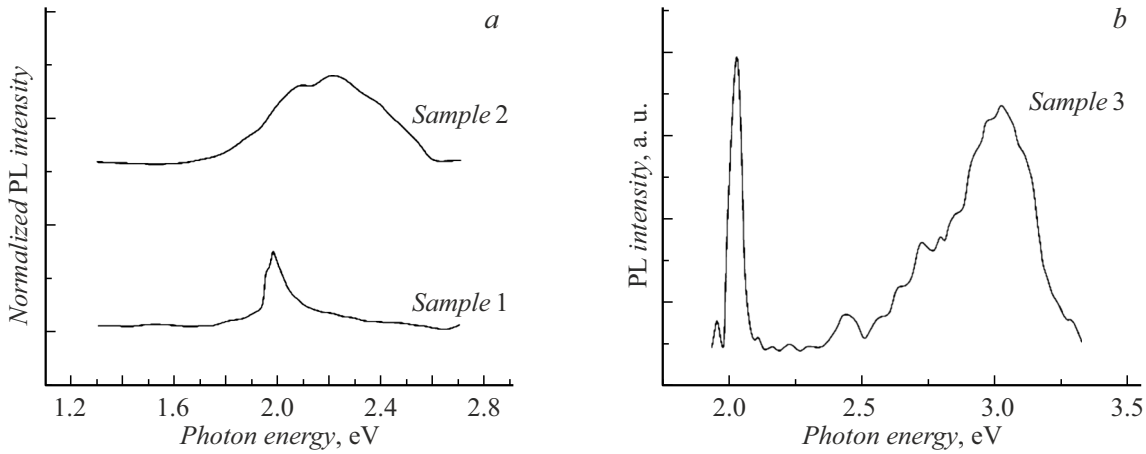

Figure 3. PL spectra of copper oxides deposited with oxygen concentration of: 1 vol.% (sample 1), 5 vol.% O_2 (sample 2), 20 vol.% O_2 (sample 3).

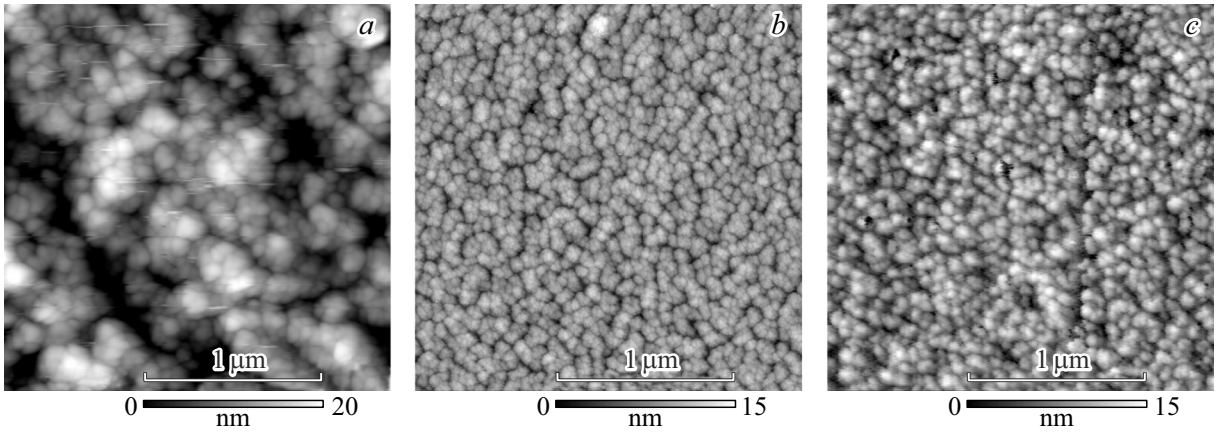

Figure 4. AFM image of the deposited Cu_2O (*a*), film topography Cu_xO (*b*), CuO (*c*).

studied in terms of exciton states (bound electron-hole pairs). Interpretation of spectra recorded at room temperature and an excitation energy much higher than the band gap is complicated by spectral noise, however, it can be observed due to high exciton binding energy. This PL band may be assigned to recombination that involves the Γ_3^- phonons of the yellow slit orthoexcitons (X_O) in Cu_2O [14]. Observed exciton peaks at 300 K indicate low density of defects ($< 10^{17}\,cm^{-3}$) and low phonon interaction energy. Anti-Stokes component is not observed at room temperature due to thermally suppressed phonon mode population. Observed exciton transition on the PL spectra indicates high crystalline quality of films with low amount of oxygen vacancies.

On the contrary, the spectrum of the samples consisting of mixed Cu_xO phases demonstrates a wide visible radiation band with its center at 2.2 eV. Due to high intensity of this band, observation of excitons becomes impossible. Notwithstanding that carrier relaxation with formation of a yellow-slit exciton takes place within a short time after generation of electron-hole pairs, a broad band in the given photon energy range dominates in the sample, which was also observed in some works [15]. Apparently, large portion of this broad band is caused by external transitions that are probably related to crystal imperfection induced by formation of the CuO phase in the film. Near these imperfections or impurity clusters, Cu_2O crystal structures get deformed and yellow and green slit symmetries may be damaged locally, thus, changing transition probabilities or even generating minor defect states in spectral regions. This facilitates the radiative recombination of electron-hole pairs in the course of relaxation to lower energy. The broad band ~ 2.2 eV may also include a contribution from interband transitions in the CuO phase ($E_g \sim 1.4$ eV) and recombination at grain boundaries.

The spectrum in Figure 3, *b* was measured on sample 3 — CuO phase. Difference from previously reviewed spectra can be seen. A sharp peak of visible orange radiation with its center at 670 nm and a broad UV peak near the band edge at 410 nm. Radiation near the band edge is assigned to radiation induced by electron and hole recombination of CuO free excitons. In CuO nanosystems, a significant part

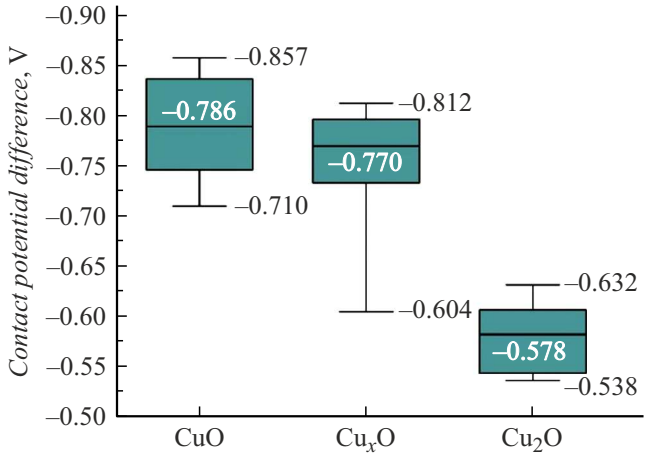

Figure 5. Distribution of CPD values with standard deviations.

of atoms resides on the surface, forming surface traps. These states generate broad spectra with high UV and visible range intensity. Spectrum of sample 3 demonstrates peaks at 350−490 nm, indicating surface states.

CuO samples may contain Cu^{+}/Cu^{2+} transition ions, that form traps for carriers and appear on radiation spectra at 500−700 nm (1.7−2.5 eV). These levels are usually in the band gap center and may induce delays in carrier relaxation. Thus, red radiation peaks (635−670 nm) may be related to the presence of copper ions with various degrees of oxidation (Cu^{+} and Cu^{2+}).

The obtained data confirms a complex behavior of defect states in the Cu_2O/CuO films and their significant influence on the carrier recombination processes. Summing up, it can be said that the samples demonstrate radiative recombination of excitons. However, film deposition conditions (partial oxygen pressure in the chamber) considerably affects the stoichiometric composition and phase homogeneity of the structure. This is reflected on PL spectra as disappearance of exciton bands and appearance of impurity bands induced by structural defects.

To obtain additional information concerning the local structure of oxide films, DC-KPFM measurements were performed. CPD is a difference in the probe tip and sample work functions. Figure 4 shows AFM images of the surface of deposited Cu_2O, Cu_xO and CuO films. Figure 5 shows the obtained values of CPD Negative values indicate that the work function of both copper oxide phases (~ 4.96 eV for Cu_2O and ~ 5.2 eV for CuO) is higher than that of the AFM silicon probe tip (~ 4.3 eV). Mean CPD for oxide previously identified as Cu_2O (sample 1) was −578 mV. While for the sample with prevailing CuO phase (sample 3), mean CPD was −786 mV. It can be seen that CPD of various phases don't overlap even at maximum deviations. Moreover, φ_{CuO} is higher than φ_{Cu2O}, which agrees with the known results [16,17]. Sample 2 containing mixed Cu_xO phases showed broad CPD distribution, which proves increased phase nonuniformity of the test sample surface. Mean value was −770 mV and was closer to CuO, which adequately agrees with our understanding of the structure of an oxide layer whose surface is easily oxidized. CPD variations may be explained by the environmental impact (measurements are carried out in air), impurities and intermediate phase inclusions.

Note that direct characterization of the degree of oxidation by comparing the theoretical and measured CPD is impossible. Deviations induced by specific sample and probe fabrication and preparation processes shall be always considered. However, relative measurements may be performed with good repeatability.

Capability of copper oxides to form stable resistive states is defined by the fact that conductive chains providing charge transfer may be formed in copper oxide structure. This process is facilitated by negatively charged copper vacancies [18] and interstitial oxygen [19] leading to formation of holes in the valence electron band. Cu^{2+} ions in CuO are in $3d^9$ states with one well localized $3d$ hole per atom. Density functional theory calculations showed that the Cu^{2+}-O_2 bond was stabilized by the Jahn-Teller distortions by means of extracting one electron from the d-state for energy minimization. Oxygen captured by surface traps in CuO generates Cu^{3+} and excess holes occurring due to the presence of Cu^{3+} induce acceptor levels higher than the valence band [20].

This causes the p-type conductivity of CuO, Cu_2O. Atomic force microscopy is an effective tool for determining resistive switching properties in a dielectric with high lateral resolution [21,22]. The cantilever needle in these measurements directly serves as an upper electrode. This allows both control of dielectric layer resistance and „reading“ the current state by setting the bias voltage to the corresponding level and polarity.

To validate AFM probe utilization as an upper electrode, „short circuit“ current and current with retracted probe were measured. Regions where the measured current was higher than 30 pA were considered to be conductive in the experiment because lower values were also observed with open circuit (current noise). Thus, experimentally found resistive states are directly related to the action of the electric field of the conductive probe. The investigation shall consider the measured current limitation related to the saturation current of the atomic-force microscope amplifier . The result is also affected by the probe tip wear and anodic oxidation reactions when investigations are performed in atmosphere.

Electrical properties of some regions of the Cu_xO film were examined by local volt-ampere characteristic (VAC) measurements ($I-V$) at room temperature. The upper electrode was grounded, and electrical bias was applied to the lower electrode. Preliminary scanning of the sample surface identified high conductivity areas. This procedure took place at a bias voltage of +10 V, therefore it was identical to an electroforming process. Later, VACs were measured after AFM probe immobilization in the chosen regions. Regions with the minimum conductive spot area

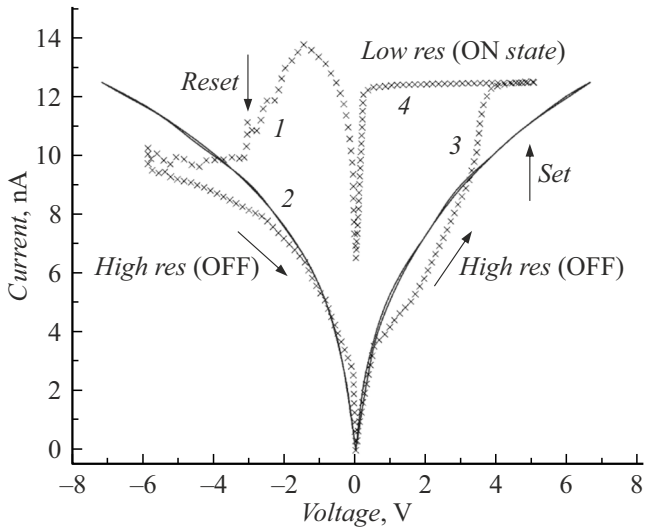

Figure 6. Typical VACs of the memristor cell: sample №2 (×) demonstrating bipolar resistive switching, and sample №3 (□) where hysteresis behavior is not observed.

were chosen for examination. The reason for this was in low current achievable in the microscope that may be insufficient to switch the formed filament with a large diameter.

Figure 6 shows a typical VAC of the given memristor cell with an interconnect layer consisting o mixed Cu_xO (sample 2). When the bias voltage was increased successively up to approximately -1.5 V, the flowing current varied stepwise. This indicates that the given film region (in the ON state with low resistance (LRS) after preliminary scanning) was switched into the OFF state with high resistance (HRS) — RESET mode (curve *1*). Curve *2* demonstrates steady decrease in current with voltage drop. Reset (SET mode — curve *3*) occurred at a voltage about $+3.5$ V, and at 4 V reached the set current limit 12.5 nA. Curve *4* shows that current remains high as voltage gradually decreases, i.e. the cell maintains low resistance, while remaining in the ON state. Five successive switching events were recorded in each of the chosen local positions. VACs of sample 1 are not shown due to high leakage currents exceeding the microscope amplifier limitation. High currents in turn may be induced by a defective structure, unoxidized copper inclusions, and high surface roughness that increased the contact area between the probe tip and sample. Sample 3 consisting of stoichiometric CuO didn't demonstrate hysteresis behavior. Thus, resistive switching is not observed in the given conditions.

Experimental results and literature data suggest that active electrode ion migration is the most probable resistive state formation mechanism in Cu_xO. Moreover, increased density of defects in the interconnect layer consisting of mixed oxides facilitates such migration (Figure 7, *a*). Lower electrode copper has ionization energy lower than that of copper in the oxide compound because higher energy is required in the ionic form (Cu^{2+} or Cu^{+}) to remove an electron than for a neutral atom. When positive bias is applied to the chemically active lower electrode, Cu^{+} are formed. These ions diffuse at oxide layer grain boundaries to the point of application of the PtIr-coated AFM probe (Figure 7, *b*). Further accumulation of ions through the layer thickness forms a conductive filament and memristor transition into the ON state with low resistance (Figure 7, *c*). Application of negative bias causes reverse drift of copper atoms along the lower electrode and filament break in its

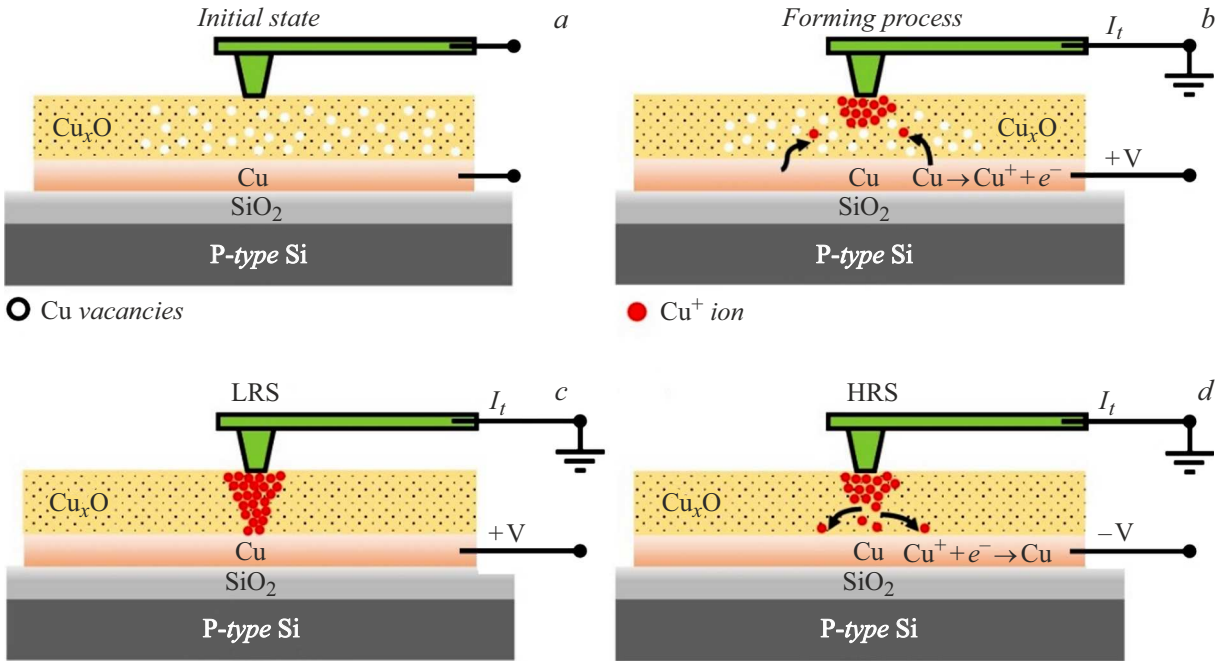

Figure 7. Schematic diagram of resistive state forming process involving a conductive filament in the Cu/CuxO/Pt-based memristor.

thinnest point, which is reflected in increasing resistance (Figure 7, *d*). The next switching on cycle takes place at a lower voltage because the filament is not fully dissolved.

Conclusion

Copper oxide thin film structures with controlled phase composition were synthesized during the study. It has been found that synthesis conditions (partial oxygen pressure) define the prevalence of the Cu_2O, CuO phases or mixture thereof, and concentration of structural defects. Probe microscopy methods have demonstrated that resistive switching in these materials was caused by a filamentary mechanism related to copper ion migration under the action of an electric field. The highest switching stability was observed in the sample with mixed phases where grain boundaries might play a significant role in forming conductive filaments as it followed from the literature data, however, localization of filaments was not reliably determined within this work.

The findings emphasize the importance of control over copper oxide defect structure and phase composition for optimizing memristor properties. Investigation of the effect of doping and electrode interface modification on long-term stability and repeatability of resistive states is a promising area of further research. The work contributes to the development of next generation energy-saving oxide-based memory devices.

Funding

The study was supported by state assignment ES-2024-0026.

Conflict of interest

The authors declare no conflict of interest.

References

[1] A.G.Isaev, O.O.Permyakov, A.E.Rogozhin. Mikroelektronika, (in Russian). **52**, 127 (2023). DOI: 10.31857/S0544126923700242
[2] C. Baeumer, R. Valenta, C. Schmitz, A. Locatelli, S.P. Rogers, A. Sala, N. Raab, S. Nemsak, M. Shim, C.M. Schneider, S. Menzel, R. Waser, R. Dittmann. ACS Nano, **11**, 6921 (2017). DOI: 10.1021/acsnano.7b02113
[3] S.M. Patil, S.S. Kundale, S.S. Sutar, P.J. Patil, A.M. Teli, S.A. Beknalkar, R.K. Kamat, J. Bae, J.C. Shin, T.D. Dongale. Sci. Reports, **13**, 4905 (2023). DOI: 10.1038/s41598-023-32173-8
[4] S. Rehman, J.-H. Hur, D.-K. Kim. J. Phys. Chem. C, **122**, 11076 (2018). DOI: 10.1021/acs.jpcc.8b00432
[5] Z. Fan, X. Fan, A. Li, L. Dong. 12th IEEE Intern., Conf. Nanotechnol. (IEEE-NANO). (Birmingham, 2012), p. 1–4, DOI: 10.1109/NANO.2012.6322196
[6] Y.-M. Hu, Z.-D. Li, C.-H. Chia, J.-W. Chiou, Y.-Y. Liao, C.-C. Yu, T.-C. Han, S.-R. Jian, J.-Y. Juang. Appl. Surf. Sci., **601**, 154215 (2022). DOI: 10.1016/j.apsusc.2022.154215
[7] U.-B. Han, J.-S. Lee. Sci. Reports, **6**, 25537 (2016). DOI: 10.1038/srep25537
[8] M. Košiček, J. Zavašnik, O. Baranov, B.Š. Batič, U. Cvelbar. Cryst. Growth & Design, **22**, 6656 (2022). DOI: 10.1021/acs.cgd.2c00863
[9] A.V. Ushakov, I.V. Karpov, L.Yu. Fedorov, E.A. Goncharova, M.V. Brungardt, V.G. Demin. ZhTF, **91** (12), 1984 (2021) (in Russian). DOI: 10.21883/JTF.2021.12.51764.157-21
[10] A.V.Ushakov, I.V.Karpov, L.Yu.Fedorov, E.A.Dorozhkina, O.N.Karpova, A.A.Shaikhadinov, V.G.Demin, A.I.Demchenko, M.V.Brungardt, E.A.Goncharova. Materialovedenie, **8**, 26 (2019). (in Russian). DOI: 10.31044/1684-579X-2019-0-8-26-32
[11] Y. Deng, A.D. Handoko, Y. Du, S. Xi, B.S. Yeo. ACS Catal., **6**, 2473 (2016). DOI: 10.1021/acscatal.6b002050
[12] L. Debbichi, M.C.M. de Lucas, J.F. Pierson, P. Krüger. J. Phys. Chem. C, **116**, 10232 (2012). DOI: 10.1021/jp303096m
[13] L.Yu.Fedorov, A.V.Ushakov, I.V.Karpov. Materialovedenie, **1**, 28 (2024). (in Russian). DOI: 10.31044/1684-579X-2024-0-1-28-34
[14] M. Takahata, N. Naka. Phys. Rev. B, **98**, 195205 (2018). DOI: 10.1103/PhysRevB.98.195205
[15] G. Martínez-Saucedo, C.G. Torres-Castanedo, S. Arias-Cerón, R. Castanedo-Pérez, G. Torres-Delgado, O. Zelaya-Ángel. J. Lumines., **215**, 116642 (2019). DOI: 10.1016/j.jlumin.2019.116642
[16] D. Nunes, T.R. Calmeiro, S. Nandy, J.V. Pinto, A. Pimentel, P. Barquinha, P.A. Carvalho, J.C. Walmsley, E. Fortunato, R. Martins. Thin Solid Films, **601**, 45 (2016). DOI: 10.1016/j.tsf.2015.11.077
[17] W. Zheng, Y. Chen, X. Peng, K. Zhong, Y. Lin, Z. Huang. Materials, **11**, 1253 (2018). DOI: 10.3390/ma11071253
[18] S. Dolai, S. Das, S. Hussain, R. Bhar, A.K. Pal. Vacuum, **141**, 296 (2017). DOI: 10.1016/j.vacuum.2017.04.033
[19] Y. Peng, Z. Zhang, T.V. Pham, Y. Zhao, P. Wu, J. Wang. J. Appl. Phys., **111**, 103708 (2012). DOI: 10.1063/1.4719059
[20] M. Younas, M. Nadeem, M. Idrees, M.J. Akhtar. Appl. Phys. Lett., **100**, 152103 (2012). DOI: 10.1063/1.3702465
[21] A.G.Isaev, O.O.Permyakov, A.E.Rogozhin. ZhTF **93**, 1143 (2023) (in Russian). DOI: 10.21883/JTF.2023.08.55976.9-23
[22] D.O.Filatov, M.N.Koryazhkina, D.A.Antonov, I.N.Antonov, D.A.Liskin, M.A.Ryabova, O.N.Gorshkov. ZhTF, **89** (11), 1669 (2019) (in Russian). DOI: 10.21883/JTF.2019.11.48326.127-19

Translated by E.Ilinskaya